Published in AIAA Journal (2019). DOI: https://doi.org/10.2514/1.J058969

Aerodynamic Characteristics of Canonical Airfoils at Low Reynolds Numbers

Karthik Menon* and Rajat Mittal†
Department of Mechanical Engineering, Johns Hopkins University, Baltimore, MD 21218, USA

I. Introduction

The aerodynamic characteristics of airfoils at low Reynolds number (Re) have been known to be markedly different from those at the high Reynolds numbers encountered in conventional air-vehicles. With recent interest in unmanned and micro-aerial vehicles, as well as bio-inspired flight, this low-Reynolds number behaviour has been garnering academic as well as practical interest. In spite of this, there is little readily available data in the literature concerning low-Reynolds number aerodynamics which are on par with high-Re datasets such as in Refs. [1, 2]. The availability of such data is important for practical design considerations as well as validation of computational models.

The distinctive behaviour of low-Re airfoil flows is primarily caused by enhanced viscous effects, and the laminar state of the flow, which leads to thicker boundary layers as well laminar flow separation [3–6]. A compilation of early measurements at low Reynolds numbers can be found in the work of Carmichael [3] and Selig *et al.* [7–9]. These measurements correspond to the regime $Re \approx 5 \times 10^4 - 5 \times 10^5$. However there have been few studies of very low-Re airfoil flows since, especially at $Re \approx 10^3$. This is in part due to the difficulty in achieving such flows in experiments, as well as the repeatability of experiments in this sensitive regime [10]. Computational modeling based studies of flow over stationary airfoils at low-Re have also been carried out, but many of these have been performed at a single angle-of-attack [11, 12]. To explore a larger portion of the parameter space, Kunz and Kroo [13] as well as Mateescu and Abdo [14] simulated low-Re airfoil aerodynamics over a large range of angles-of-attack, Reynolds numbers and airfoil shape. However, they employed *steady models* that ignore unsteady effects such as vortex shedding. More recently, Kurtulus [15] studied the flow over a NACA 0012 airfoil over a range of angles-of-attack at $Re = 1000$ using time-resolved simulations. In another study, Liu *et al.* [16] analyzed static and dynamic stall of a NACA 0012 airfoil at $Re = 1000$. Both of these studies provide time-resolved aerodynamic quantities at low-Re, however, they have been performed for a single airfoil shape and Re. The effect of airfoil shape at a single Reynolds number of $Re = 1000$ was investigated in a recent study by Meena *et al.* [17], where the focus was on the effect of a Gurney flap on the wake behind the airfoil.

In this Note we describe results from two-dimensional simulations of low-Re flow ($500 \leq Re = U_\infty C/\nu \leq 2000$) over three different NACA airfoils, obtained using highly-resolved, unsteady incompressible Navier-Stokes simulations.

*Graduate Student; Email: kmenon@jhu.edu
†Professor; Email: mittal@jhu.edu

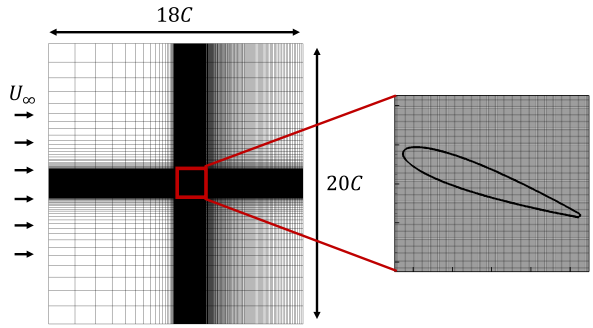

Fig. 1 Computational domain and grid used in the present study.

The aim of this work is to provide a comprehensive database of the variation in key aerodynamics quantities (force coefficients, center-of-pressure and Strouhal numbers) with Reynolds number, angle-of-attack and airfoil shape. This data should provide an improved understanding of airfoil aerodynamics at these very low Reynolds numbers and also serve as a database for validation of computational models.

II. Computational Method

We simulate the flow using a sharp-interface immersed-boundary method of Mittal *et al.* [18, 19]. This method allows us to preserve sharp interfaces along the surface of our geometry using a non-conformal Cartesian grid. The unsteady, incompressible Navier-Stokes equations are solved using a fractional-step method, and the pressure Poisson equation is solved using the geometric multigrid method. All spatial derivatives use second-order finite differences, and time integration is performed using a second-order Adams-Bashforth method. The method is second-order in space and time. Extensive validation of this method for a variety of flows can be found in Mittal *et al.* (2008) [18]. Further, we have made comparisons of the lift coefficient and frequency of lift oscillations estimated from this work with published literature [15, 16], and have shown good agreement. These comparisons are shown in figures 4, in section III.C.

III. Results

The airfoils used here are from the NACA family: NACA 0012, NACA 0015 and NACA 4415. The airfoil (chord length C) is immersed in a domain of size $18C \times 20C$, and a non-uniform Cartesian grid with 480×448 points is employed. A schematic of this is shown in figure 1. All reported quantities are scaled using the fluid density (ρ), freestream velocity (U_∞), and chord length (C) as characteristic scales. Grid convergence is assessed by simulating the airfoil flow at $Re = 2000$ with grid sizes of 384×320, 480×448 (baseline used in this study), and 544×544. The mean and RMS C_L differ by 4.1% and 1.2% respectively between the coarse and baseline grids, and 4.8% and 0.3% respectively between the fine and baseline grids. The difference in mean and RMS C_M is 2.7% and 1.2% between the coarse and baseline grids, and 1.8% and 0.9% between the fine and baseline grids. Thus, the computed quantities are

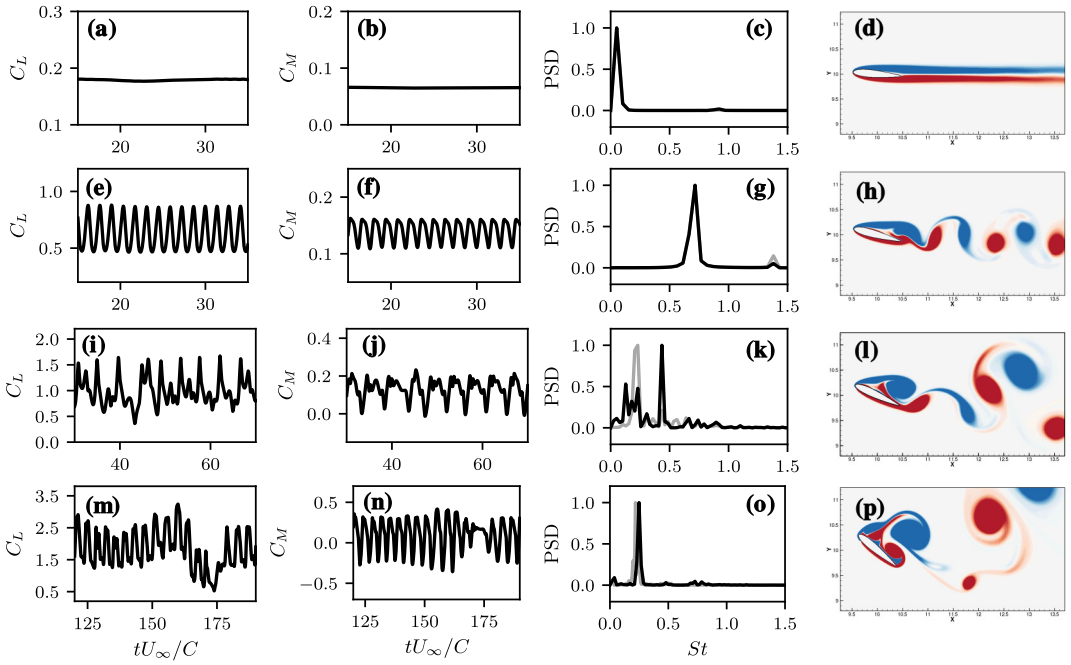

Fig. 2 C_L **(leftmost pane) and** C_M **(middle-left pane) time-series plots, frequency spectra of** C_L **and** C_M **(middle-right pane), and snapshots of vorticity fields (rightmost pane) for different regimes of unsteady behaviour at** $Re = 1000$**. Frequency spectra are shown in terms of** St**, with the black and grey lines showing the spectra of** C_L **and** C_M **respectively, each scaled by the magnitude of the peak for clarity. (a)-(d)** $\alpha = 5°$**; (e)-(h)** $\alpha = 15°$**; (i)-(l)** $\alpha = 25°$**; (m)-(p)** $\alpha = 40°$**.**

considered grid independent.

As will become apparent in the next section, these low-Reynolds number flows over airfoils may be unsteady and also not strictly periodic. Well converged statistics therefore necessitate very long integration times ($c/U_\infty \sim 150 - 250$), which translates to $3 - 5 \times 10^5$ time-steps in our simulations. Thus, even these two-dimensional simulations require significant computational resources. Each simulation has been performed on 210 processors and required approximately 48 hours to turn around. Result from a total of 72 simulations are reported here.

A. Flow regimes

We begin with a qualitative discussion of the flow behaviour observed at different angles-of-attack for the NACA 0015 airfoil at $Re = 1000$. We see that the wake behind the airfoil transitions from a steady wake, to a Karman vortex street, and finally to a leading-edge vortex (LEV) dominated flow as the angle-of-attack is increased well past the static stall angle. The steady, pre-vortex shedding regime is shown in figures 2(a)-(d), for $\alpha = 5°$. Figures 2(e)-(h) correspond to $\alpha = 15°$ where periodic oscillations in C_L and C_M result from the Karman vortex shedding. Figures 2(i)-(l) show the behaviour at $\alpha = 25°$, where the C_L and C_M time-series show low as well as high-frequency components due to a 1P-1S (one vortex pair and single vortex) shedding mode. The high-frequency mode corresponds to Karman vortex-shedding, and the formation and shedding of the LEV causes the low-frequency oscillations. In figure 2(m)-(p)

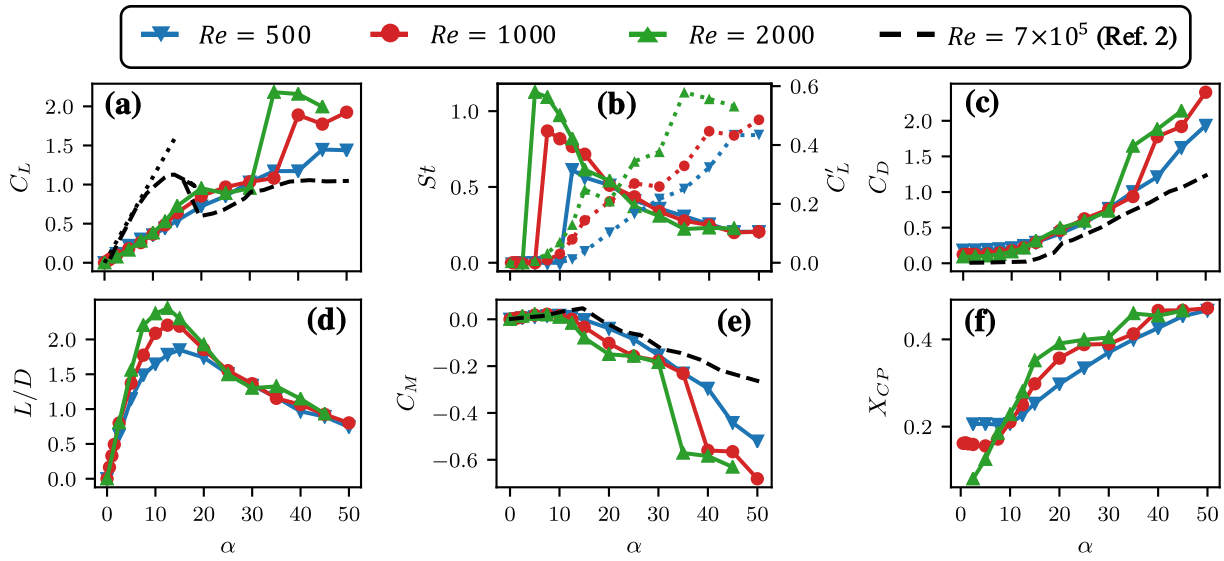

Fig. 3 Aerodynamic quantities for the NACA 0015 airfoil for $Re = 500, 1000, 2000$. Dashed line shows experimental measurements at Re=7×10^5 from Ref. [2]. (a) Coefficient of mean lift, C_L. Dotted line indicates $C_L = 2\pi\alpha$.; (b) Strouhal number (St; solid lines) and standard deviation (C'_L; dotted lines) of C_L oscillations; (c) Coefficient of mean drag, C_D; (d) Lift-to-drag ratio.; (e) Coefficient of mean moment about quarter-chord, C_M; (f) Mean location of center-of-pressure, X_{CP}.

we see the characteristics of the $\alpha = 40°$ case which are dominated by the low-frequency shedding of a large LEV and a small TEV. The time-variations of the coefficients for this case also exhibits stochastic variations interspersed with quasi-periodic behavior. The complex behavior of the flow at these low Reynolds numbers is due to the simultaneous presence of a number of length scales of comparable magnitude such as the chord length, the airfoil thickness, the frontal projected height of the airfoil and the thicknesses of the boundary layer on the suction and pressure surfaces of the airfoil. Further, the non-periodic nature of the flow for the high angle-of-attack cases necessitates extremely long integration times to accumulate reliable statistics.

B. Effect of Reynolds Number

Figure 3 shows a comparison of computed force coefficients for the NACA 0015 airfoil at $Re = 500, 1000$ and 2000, as a function of angle-of attack, α. These are also compared with the high-Re experimental measurements of C_L, C_D and C_M from Sheldahl and Klimas at $Re = 7 \times 10^5$ [2]. Figure 3(a) shows the trend for mean C_L. At low α, the mean C_L is similar for the three values of Re, and the lift-slope is about half of the theoretical value of 2π as well as the slope at high Reynolds number (7×10^5). The mean C_L increases monotonically for $Re = 500$ and 1000, whereas there is a mild stall at $20° \leq \alpha \leq 25°$ for $Re = 2000$. However none of the cases shows any indication of the deep stall apparent for the high Reynolds number case. Also contrary to the high-Re behaviour, all three cases exhibit a significant increase in mean C_L for approximately $\alpha \geq 35°$. This increase is caused by the formation and shedding of a leading-edge vortex and the magnitude of this jump in mean C_L is found to increase with Reynolds number.

Figure 3(b) highlights the unsteady nature of C_L, with the standard deviation of C_L plotted using dotted lines and the Strouhal number (St) of lift oscillations plotted using solid lines. At low angles, St is zero due to the flow being steady, as seen in figures 2(a)-(c). This is followed by a jump in St as α is increased, which corresponds to the onset of unsteady vortex shedding, followed by a monotonic decrease in St. We see that the onset of unsteadiness ranges from $\alpha \approx 12.5°$ for Re=500 to $\alpha \approx 5°$ for Re=2000. It is noted that figure 3(b) shows the most dominant frequency, however at high angles-of-attack ($\alpha > 25°$) the lift oscillations exhibit multiple frequencies, as seen in figure 2. The intensity of C_L fluctuations are captured by the standard deviation, C_L'. The $Re = 500$ and 1000 cases show a mostly monotonic increase in the intensity of lift fluctuations with α, but the $Re = 2000$ case shows a complex non-monotonic behavior.

The behaviour of C_D, shown in figure 3(c), is unremarkable except for jump in the value beyond $\alpha \approx 20°$ for the two higher Reynolds number cases. It must also be noted that as expected, the drag in these cases is larger than that at high-Re. Figure 3(d) shows the lift-to-drag ratio for these cases. The peak in C_L/C_D occurs between $\alpha \approx 15°$ for $Re = 500$, and $\alpha \approx 10°$ for $Re = 2000$. Also, we see that the peak lift-to-drag ratio at these low Reynolds numbers is significantly lower than those at much higher Reynolds number used in conventional aerospace applications, which can be in the range $C_L/C_D \approx 20 - 50$ at high Reynolds numbers [2].

Figure 3(e) shows C_M and we see that at small α the moment is close to zero and shows very small variation with α. This is one feature that these low-Reynolds numbers flows appear to share with their higher Reynolds number counterparts. The magnitude of C_M increases with Re at high α, and is negative for $\alpha > 10°$. This is related to a shift in the center-of-pressure, which we plot in figure 3(f). We see that X_{CP} stays constant for small angles at lower Re, with this value being farther downstream for lower Re. On increasing α we see that X_{CP} moves downstream, reaching close to mid-chord at $\alpha = 50°$.

C. Effect of Airfoil Shape

We now briefly describe the effect of shape on the aerodynamic characteristics by comparing the simulation data for NACA 0012, NACA 0015, and NACA 4415 airfoils at $Re = 1000$. Figure 4(a) shows that the NACA 4415 produces a small but measurable negative lift at $\alpha = 0°$ and this unusual effect is contrary to what is observed at conventional Reynolds numbers (see Ref. [1]). In fact, such peculiar behaviour at low-Re has been previously reported at small angles-of-attack [10]. The lift for the NACA 4415 also increases more rapidly with angle-of-attack compared to the other airfoils, leading to a larger mean lift at the intermediate angles-of-attack. The other significant difference amongst the three airfoils is in the lift-to-drag ratio and the center-of-pressure. The NACA 4415 airfoil generates the largest value of C_L/C_D which is about 32% higher than the NACA 0015 airfoil. The center-of pressure of the NACA 4415 airfoil is also quite disparate from the other two airfoils for $\alpha < 15°$. Also shown in figure 4(a) and (b) are comparisons of the mean and Strouhal number of C_L fluctuations computed in this work for a NACA 0012 airfoil at $Re = 1000$ (purple line) with the results of Kurtulus [15] (dashed line) and Liu *et al.* [16] (dash-dotted line). We note that the comparison

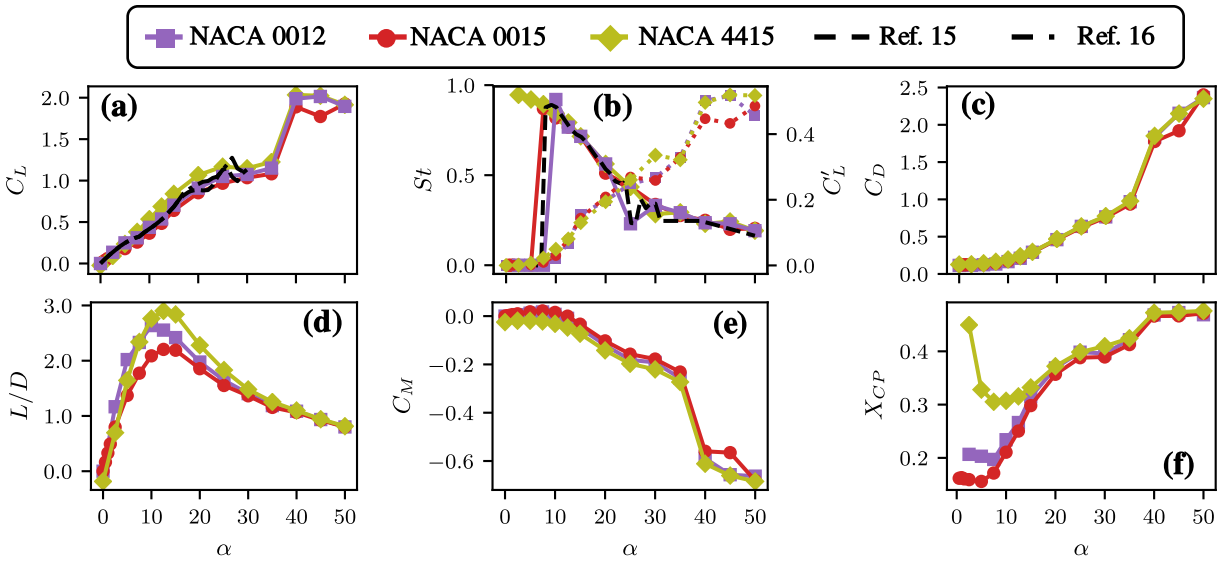

Fig. 4 Force coefficients as a function of angle-of-attack (α) for three airfoil shapes at Re=1000. The dashed line shows measurements from Kurtulus [15] and Liu *et al.* [16]. (a) Coefficient of mean lift, C_L. Dotted line indicates $C_L = 2\pi\alpha$.; (b) Strouhal number (St; solid lines) and standard deviation (C'_L; dotted lines) of C_L oscillations; (c) Coefficient of mean drag, C_D; (d) Lift-to-drag ratio.; (e) Coefficient of mean moment about quarter-chord, C_M; (f) Mean location of center-of-pressure, X_{CP}.

for both these quantities is quite good.

IV. Conclusion

Using highly-resolved, unsteady incompressible flow simulations, we have catalogued the aerodynamic performance of three NACA airfoils - NACA 0012, NACA 0015, NACA 4415 - at $Re = 500, 1000$ and 2000 and angles-of attack ranging from $0° \leq \alpha \leq 50°$. Despite the low Reynolds number and laminar nature of the flow, the flow exhibits significant complexity due to the presence of distinct flow phenomena such as Karman vortex shedding as well as leading-edge vortex (LEV) formation and shedding. This leads to large and rapid changes in the measured quantities with angle-of-attack. The effect of airfoil shape appears primarily in the lift-to-drag ratio and the center-of-pressure. Taken together, these results provide an overview of the complexity of these laminar airfoil flows and also provide a comprehensive database for the validation of computational models. In terms of the limitations of this work, the flow is expected to exhibit intrinsic three-dimensionality when the Reynolds number based on the frontal projection exceeds approximately 200. Thus, for a large range of the parameter space simulated here, three-dimensional effect could modify the flow and the aerodynamics quantities. Extension of this study to three-dimensional simulations would therefore be insightful but would also require significantly more computational resources.

Acknowledgments

This work is supported by the Air Force Office of Scientific Research under Grant Number FA 9550-16-1-0404, monitored by Dr. Gregg Abate.

References

[1] Abbott, I. H., and Von Doenhoff, A. E., *Theory of wing sections, including a summary of airfoil data*, Courier Corporation, 1959.

[2] Sheldahl, R. E., and Klimas, P. C., "Aerodynamic characteristics of seven symmetrical airfoil sections through 180-degree angle of attack for use in aerodynamic analysis of vertical axis wind turbines," Tech. rep., Sandia National Laboratories (SNL), Albuquerque, NM, and Livermore, CA (United States), 3 1981. doi:10.2172/6548367, URL http://www.osti.gov/servlets/purl/6548367/.

[3] Carmichael, B. H., "Low Reynolds number airfoil survey, volume 1," *NASA Contractor Report 165803*, Vol. 1, 1981. URL https://ntrs.nasa.gov/search.jsp?R=19820006186.

[4] Lissaman, P. B. S., "Low-Reynolds-Number Airfoils," *Ann. Rev. Fluid Mech*, Vol. 15, 1983, pp. 223–239. doi:10.1146/annurev.fl.15.010183.001255, URL https://www.annualreviews.org/doi/abs/10.1146/annurev.fl.15.010183.001255?journalCode=fluid.

[5] Mueller, T. J., and DeLaurier, J. D., "Aerodynamics of Small Vehicles," *Annual Review of Fluid Mechanics*, Vol. 35, No. 1, 2003, pp. 89–111. doi:10.1146/annurev.fluid.35.101101.161102, URL http://www.annualreviews.org/doi/10.1146/annurev.fluid.35.101101.161102.

[6] Shyy, W., Lian, Y., Tang, J., Viieru, D., and Liu, H., *Aerodynamics of low Reynolds number flyers*, Vol. 22, Cambridge University Press, 2007.

[7] Selig, M., Guglielmo, J., Broeren, A., and Giguère, P., *Summary of Low-Speed Airfoil Data, Vol. 1*, SoarTech Publications, Virginia Beach, VA, 1995.

[8] Selig, M., Lyon, C., Giguère, P., Ninham, C., and Guglielmo, J., *Summary of Low-Speed Airfoil Data, Vol. 2*, SoarTech Publications, Virginia Beach, VA, 1996.

[9] Lyon, C., Broeren, A., Giguère, P., Gopalarathnam, A., and Selig, M., *Summary of Low-Speed Airfoil Data, Vol. 3*, SoarTech Publications, Virginia Beach, VA, 1997.

[10] Tank, J., Smith, L., and Spedding, G. R., "On the possibility (Or lack thereof) of agreement between experiment and computation of flows over wings at moderate Reynolds number," *Interface Focus*, Vol. 7, No. 1, 2017. doi:10.1098/rsfs.2016.0076, URL https://royalsocietypublishing.org/doi/pdf/10.1098/rsfs.2016.0076.

[11] Mittal, S., and Tezduyar, T. E., "Massively parallel finite element computation of incompressible flows involving fluid-body interactions," *Computer Methods in Applied Mechanics and Engineering*, Vol. 112, No. 1-4, 1994, pp. 253–282. doi: 10.1016/0045-7825(94)90029-9, URL http://citeseerx.ist.psu.edu/viewdoc/download?doi=10.1.1.738.3745&rep=rep1&type=pdf.

[12] Jones, L. E., Sandberg, R. D., and Sandham, N. D., "Direct numerical simulations of forced and unforced separation bubbles on an airfoil at incidence," *Journal of Fluid Mechanics*, Vol. 602, 2008, pp. 175–207. doi:10.1017/S0022112008000864, URL https://doi.org/10.1017/S0022112008000864.

[13] Kunz, P. J., and Kroo, I. M., "Analysis, Design, and Testing of Airfoils for Use at Ultra- Low Reynolds Numbers," *Fixed Flapping and Rotary Wing Aerodynamics for Micro Aerial Vehicle Applications*, 2001, pp. 35–60. URL http://aero.stanford.edu/Reports/NDPAPER_kunz.pdf.

[14] Mateescu, D., and Abdo, M., "Analysis of flows past airfoils at very low Reynolds numbers," *Proceedings of the Institution of Mechanical Engineers, Part G: Journal of Aerospace Engineering*, Vol. 224, No. 7, 2010, pp. 757–775. doi:10.1243/09544100JAERO715.

[15] Kurtulus, D. F., "On the Unsteady Behavior of the Flow around NACA 0012 Airfoil with Steady External Conditions at Re=1000," *International Journal of Micro Air Vehicles*, Vol. 7, No. 3, 2015, pp. 301–326. doi:10.1260/1756-8293.7.3.301, URL https://journals.sagepub.com/doi/pdf/10.1260/1756-8293.7.3.301.

[16] Liu, Y., Li, K., Zhang, J., Wang, H., and Liu, L., "Numerical bifurcation analysis of static stall of airfoil and dynamic stall under unsteady perturbation," *Communications in Nonlinear Science and Numerical Simulation*, Vol. 17, No. 8, 2012, pp. 3427–3434. doi:10.1016/j.cnsns.2011.12.007, URL https://linkinghub.elsevier.com/retrieve/pii/S1007570411006666.

[17] Meena, M. G., Taira, K., and Asai, K., "Airfoil-wake modification with Gurney flap at low reynolds number," *AIAA Journal*, Vol. 56, No. 4, 2018, pp. 1–12. doi:10.2514/1.J056260.

[18] Mittal, R., Dong, H., Bozkurttas, M., Najjar, F. M., Vargas, A., and von Loebbecke, A., "A versatile sharp interface immersed boundary method for incompressible flows with complex boundaries," *Journal of Computational Physics*, Vol. 227, No. 10, 2008, pp. 4825–4852. doi:10.1016/j.jcp.2008.01.028.

[19] Seo, J. H., and Mittal, R., "A sharp-interface immersed boundary method with improved mass conservation and reduced spurious pressure oscillations," *Journal of Computational Physics*, Vol. 230, No. 19, 2011, pp. 7347–7363. doi:10.1016/j.jcp.2011.06.003, URL http://linkinghub.elsevier.com/retrieve/pii/S0021999111003524.